Scientific paper

Laser Control of Single and Double Proton Transfer Reactions

Nada Došlić,[1,*] Mahmoud K. Abdel-Latif[2,3] and Oliver Kühn[2,*]

[1] *R. Bošković Institute, Bijenička 54, 10000 Zagreb, Croatia*

[2] *Institute of Physics, University of Rostock, D-18051 Rostock, Germany*

[3] *Chemistry Department, Faculty of Science, Beni-Suef University, Beni-Suef, Egypt*

* *Corresponding author: E-mail: nadja.doslic@irb.hr, oliver.kuehn@uni-rostock.de*

Received: 29-03-2011

Dedicated to Professor Dušan Hadži on the occasion of his 90th birthday

Abstract

Theory and simulation of laser control of single and double proton transfer reactions in hydrogen-bonded molecular systems are reviewed. Different approaches to the construction of potential energy surfaces are introduced as a means to design simple models for unraveling basic mechanistic principles of laser control. Obtaining the control laser field is the central task and various methods such as optimal control theory are outlined. Applications are presented for the infrared laser-driven single proton transfer in models of thioacetylacetone and acetylacetone as well as for the double proton transfer in porphycene derivatives.

Keywords: Hydrogen bonds, laser control, single proton transfer, double proton transfer

1. Introduction

Single and multiple hydrogen bonds (HBs) and related proton or H atom transfer are of fundamental importance in Chemistry and Biology.[1,2] Therefore, it is not surprising that the development of the field of laser control from theoretical model simulations in the 1980s to a versatile tool for manipulating chemical reaction dynamics (for an overview see, e.g., Ref. 3) has also triggered efforts to achieve control of proton or H atom dynamics in HBs.[4,5] Besides being of importance for potential applications, HBs pose some fundamental challenges due to the strongly anharmonic[6] and multidimensional quantum character of their dynamics.[7] In fact since existing strategies for laser control of HBs often operate in the infrared (IR) domain, they share difficulties with conventional simulations of IR spectral line shapes.[8] The first proposal for IR laser control of an intra-molecular proton transfer (PT) reaction has been made for a two-dimensional (2D) model of a malonaldehyde derivative[9], adapting the pump-dump scheme developed for other isomerization reactions (see, e.g., Ref. 10). Subsequently, optimal control theory (OCT) has been applied to PT discovering the so-called "hydrogen subway" mechanism, which operates by driven proton tunneling.[11] This mechanism has been explored further to include dissipation effects,[12–15] and to clarify its spectroscopic observation.[16,17] Moreover, the implications of the sub-cycle nature of the control pulses have been investigated.[18,19] There have also been a few other reports on laser control of PT, i.e. exploring the role of pure dephasing,[20] applying local control theory,[21] and demonstrating quantum computer operations using double minimum potentials.[22] Recently, there has been some interesting discussion of PT control in enzymes, where the laser excitation is designed such as to enhance tunneling.[23]

Double hydrogen bonds and related double proton or H atom transfer (DPT) reactions, although representing the simplest case of multi-HB dynamics, already provide a wealth of new phenomena as compared to single HBs due to the possibility of correlated particle dynamics. Having two protons there are in principle two possible mechanisms for DPT as sketched in Figure 1. Either both protons move concertedly (synchronous) passing a highly symmetric transition state (usually a second order saddle

point) or they move step-wise (asynchronous) through transition states of lower symmetry and passing an intermediate local minimum on the potential energy surface (PES). Despite the simplicity of this classification, an experimental elucidation of the mechanism for specific systems appears to be quite challenging as is illustrated by the controversial discussion of the excited state DPT in the dimer formed by 7-azaindole, a DNA base pair mimicking complex.[24–30] An important issue in this respect is the time scale and type of vibrational motions of the whole molecule, which are coupled to the DPT reaction. In particular under thermal conditions this requires a "softening" of the strict symmetry criterion for assignment of a concerted mechanism. Related studies employing classical trajectories can be found for the formic acid dimer in Ref. 31 and for porphycene in Ref. 32. A recent quantum dynamical simulation on a 2D model for porphine gave still another perspective on this issue:[33] Upon excitation of the ground state wave packet, describing the DPT coordinates, above the barrier for concerted DPT, the mechanism might change from concerted to step-wise as a consequence of the wave packet reflection on the repulsive wall of the product range of the PES.

In the electronic ground state the situation is even more complicated due to the fact that DPT is not easily triggered in common spectroscopic experiments. Therefore, the mechanism of DPT is commonly inferred from line splittings in absorption spectra[34,35] or thermal rate constants. However, a decision based on rate constants is often not that clear-cut[36] and it may depend on the experimental conditions such as temperature.[37]

Similar to single HB systems, the DPT dynamics will be coupled to vibrational motions of the molecular scaffold.[7] There is ample evidence that vibrational motion can have a promoting (see, e.g., porphycene in Refs. 32, 34 and 35) or inhibiting effect (see, e.g., formic acid dimer in Refs. 38–41) on DPT. Viewed from a dynamical perspective, correlated motion, which compresses and expands the two HBs in-phase is likely to trigger concerted DPT, whereas an anti-correlated out-of-phase dynamics will be favorable for step-wise transfer (see Figure 1). In passing we note that the methods of multidimensional IR spectroscopy are capable of unraveling this dynamics for systems as complex as nucleic acid base pairs in solution.[42] Still another perspective on the behavior of DPT systems is provided by NMR spectroscopy. Limbach and coworkers, by combining NMR chemical shift data and quantum mechanical calculations of nuclear ground state probability distributions, showed that a connection between H/D isotope effects and the mechanism of DPT can be established.[43,44] Specifically, the interplay of anharmonic couplings and mass-dependent zero-point energy has an effect on the geometry that can be explored to find the degree of cooperativity of the two HBs in the vicinity of the global minima on the PES, however, without having at hand a conclusion on the transfer mechanism.

Laser control of DPT reactions have not attracted much attention so far. There are several reports, which share the assumption that the transfer mechanism was fixed *a priori*. For instance, Nishikawa *et al.* considered control of stepwise DPT in an asymmetrically substituted tetraflouro-porphyrin model using the stimulated Raman adiabatic passage (STIRAP) method.[45] Assuming a stepwise transfer, the description has been reduced to two independent one-dimensional potentials obtained from intrinsic reaction coordinate calculations. It was shown that STIRAP could achieve population inversion related to stepwise DPT on a time scale of some tens of picoseconds.

Shapiro and coworker have investigated DPT in the context of DNA radiation damage and repair for a dinucleotide model.[46] They developed a 2D PES for DPT comprising a linear reaction coordinate for the concerted DPT supplemented by an out-of-plane squeezing type vibrational mode. Employing coherently controlled adiabatic passage, detection and repair of DPT related mutation has

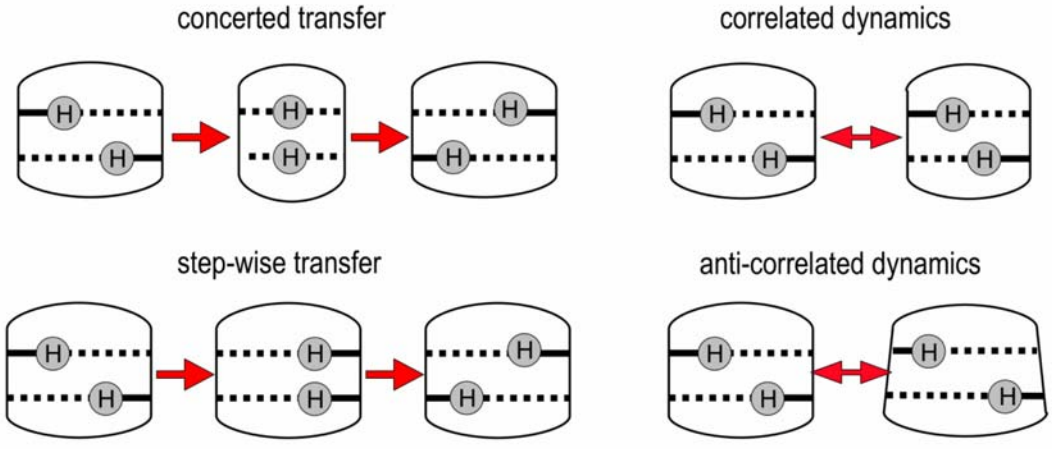

Figure 1. Left panel: Concerted vs. step-wise DPT via a second order saddle point and a stable intermediate, respectively. Right panel: Correlated dynamics compresses and expands both HBs in-phase, whereas in anti-correlated dynamics this motion is out-of-phase.

been demonstrated. Thanopulos *et al.* have discussed the implications of DPT control for single molecule charge transfer.[47] Considering a thio-functionalized porphyrin derivative attached to four gold electrodes it was found from molecular orbital analysis that the different *trans* forms essentially provide orthogonal pathways for electron transfer. Laser controlled switching was discussed in a step-wise model comprising two bond coordinates for the first step and a single linear reaction coordinate for the second one. An overview of this work can be found in Ref. 48.

Recently, we have investigated laser control of DPT in a 2D model comprising both, concerted and step-wise pathways.[49,50] Different control strategies have been found to successfully switch between the two *trans* forms of models mimicking porphycene derivatives. In contrast to situations being relevant for ground state kinetics and in similarity to the study of Manz and coworkers,[33] we have found that laser-driven DPT carries the system far away from the equilibrium and minimum energy pathways, such that the distinction between concerted and step-wise transfer becomes difficult, if not meaningless.

This paper reviews the state of affairs concerning the laser control of single and double proton transfer reactions. It is organized as follows: In Section 2 theoretical models for the description of these reactions will be introduced and some remarks on the numerical solution of the time-dependent Schrödinger equation will be given. Section 3 is devoted to a brief review on methods for laser pulse design. Application for PT and DPT control are given in Section 4 and some final remarks follow in Section 5.

2. Model Hamiltonian and Equations of Motion

2. 1. Single Proton Transfer

A simple 2D model of the intra-molecular PT in thioacetylacetone has been put forward in Ref. 12. (Note that in the present context, no distinction between electronic species is made and the term PT is used throughout although some of the reactions could be classified at H atom transfer.) Although it cannot fully account for the complexity of the actual reaction, it allows uncovering some key aspects of laser-driven PT. The Hamiltonian has all-Cartesian character and is formulated in terms of a PT reaction coordinate x (mass m_x) and an orthogonal normal mode coordinate Q (mass m_Q) mimicking the effect of the heavy atom rearrangement of the molecular scaffold upon PT due to anharmonic couplings. Thus the Hamiltonian takes the form

$$H_0 = \frac{p_x^2}{2m_x} + \frac{p_Q^2}{2m_Q} + V_x(x) + V_Q(x,Q)\,. \tag{1}$$

For the double minimum potential along the x coordinate one can start with two shifted harmonic diabatic potentials $V_i^{(\mathrm{osc})}(x) = \frac{k_i}{2}(x - x_{0,i})^2 + \Delta_i$ (i = 1,2 corresponding to reactant and product configuration), which are coupled by means of a Gaussian coupling function $K(x) = k_c \exp\{-(x - x_c)^2\}$. Diagonalizing this two state problem, the PES for the PT coordinate follows from the lower root as

$$V_x(x) = \frac{1}{2}\left[V_1^{(\mathrm{osc})}(x) + V_2^{(\mathrm{osc})}(x) - \sqrt{\left[V_1^{(\mathrm{osc})}(x) - V_2^{(\mathrm{osc})}(x)\right]^2 + 4K^2(x)} \right]. \tag{2}$$

The heavy atom coordinate is incorporated using a locally harmonic potential of the form

$$V_Q(x,Q) = \frac{k_Q}{2}\left[Q - f(x)\right]^2 . \tag{3}$$

For the case of thioacetylacetone the index i = 1 and 2 refers to the enol and enethiol form, respectively. The asymmetry of this PES can be taken into account through the coupling function $f(x) = ax^2 + bx^3$ in Equation (3). In an analogous way the dipole moment operator $\mu(x,Q)$ can be fitted to incorporate the changes of the dipole moment from 4.27 D in the enol form to 3.65D in the enethiol form. This enables expressing the interaction of the molecule with a laser field $E(t)$ in the semiclassical form (assuming that dipole moment and field are parallel)

$$H_{\mathrm{field}}(t) = -\mu(x,Q)E(t)\,. \tag{4}$$

The resulting PES is shown in Figure 2. It has been obtained by fitting MP2/6-31+G(d,p) data computed for the two minima and the transition state in Ref. 12. Figure 2 also contains some of the lowest eigenfunctions of H_0 which have been obtained by solving the time-independent Schrödinger equation

$$H_0\phi_v(x,Q) = E_v\phi_v(x,Q) \tag{5}$$

using the Fourier Grid Hamiltonian (FGH) method.[51] The two lowest eigenfunctions ϕ_0 and ϕ_1 correspond to the enol and enethiol form of thioacetylacetone. The next state ϕ_2 is the fundamental excitation of the heavy atom mode in the enol form. Finally, we show ϕ_8 which is energetically above the reaction barrier and delocalized along the PT coordinate. From Figure 2 it is apparent that the laser-driven PT from the enol to the enethiol minimum corresponds to the population inversion between the ground state ϕ_0 and the first excited state ϕ_1. Note, that the splitting of the lowest doublet in our model system is 176 cm^{-1}. This is in accord with the well-known rapid inter-conversion of the enol and enethiol tautomeric forms.[52]

The simple model discussed so far, while illustrative has severe drawbacks. It is well know that PT is a truly multidimensional reaction involving collective large amplitude motions.[7] Hence methods capable of constructing

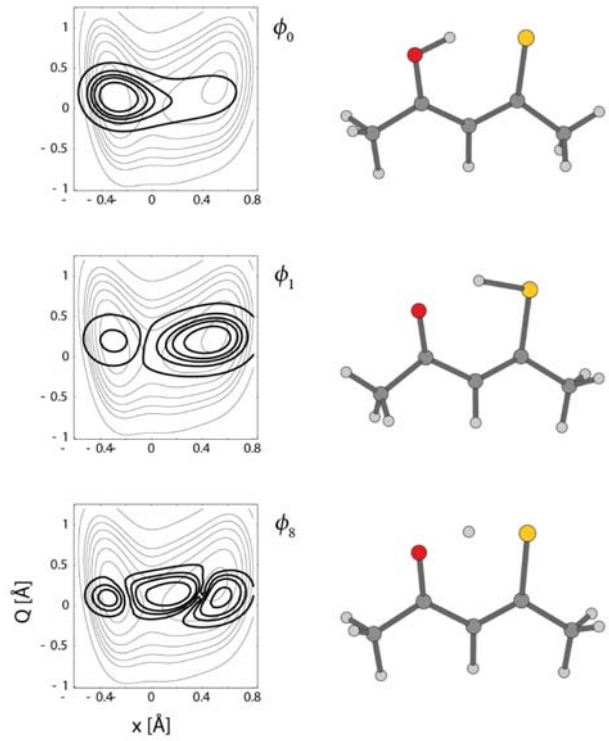

Figure 2. The 2D PES for PT (actually H-atom transfer, *cf.* Ref. 12) in thioacetylacetone is shown together with the density plots of vibrational eigenstates: ϕ_0, ϕ_1, and ϕ_8. The more stable enol configuration corresponds to the left-hand side minimum. The parameters of the potential are: $x_{0,1} = -0.38$ Å, $x_{0,2} = 0.64$ Å, $\Delta_1 = 0$, $\Delta_2 = 0.0975$ eV, $k_c = 4.24$ eV, $x_c = 0.152$ Å, $k_1 = 5.95$ mdyne/Å, $k_2 = 4.31$ mdyne/Å eV, $a = 1.5$ Å^{-1}, $b = -0.96$ Å^{-2}.

more accurate PES need to be considered.[53,54] One approach, which retains the simplicity of laser control within the H-bonding moiety by describing the PT reaction in non-orthogonal internal coordinates has been put forward in Refs. 55–57. We shall describe the approach using the example of acetylacetone (2,4 dioxopentane), a prototype system for intramolecular HBs.[58] The PES is constructed in terms of three large amplitude coordinates, $\rho_1 = r_1 + r_2$, $\rho_3 = r_1 - r_2$, and $\rho_3 = \theta$, where r_1 is the distance between the hydrogen and the donor oxygen, r_2 is the distance from the hydrogen to the acceptor oxygen atom, and θ is the OHO angle. In terms of (ρ_1, ρ_2, ρ_3) the molecular Hamiltonian reads

$$H_0 = -\frac{\hbar^2}{2}\sum_{r=1}^{3}\sum_{s=1}^{3}\frac{\partial}{\partial\rho_r}\left[G^{rs}\frac{\partial}{\partial\rho_s}\right]+V(\rho_1,\rho_2,\rho_3), \quad (6)$$

where the kinetic energy matrix elements G^{rs} are given by

$$G^{rs} = \sum_{i=1}^{3N}\frac{1}{m_i}\frac{\partial\rho_r}{\partial x_i}\frac{\partial\rho_s}{\partial x_i} \quad (7)$$

and $\{x_i\}$ denotes the set of $3N$ Cartesian coordinates. In other words, within this approach the kinetic energy matrix **G** accounts for the coupling of the H-bonding fragment to the remaining molecular coordinates.

2. 2. Double Proton Transfer

In the following we will outline a simple yet insightful model for a DPT Hamiltonian, which originally had been proposed by Smedarchina and coworkers (see, e.g.,[59,60] and for a review Ref. 61). Its physical meaning can be appreciated by starting from a linear arrangement of two HBs (cf. Figure 1), where the motion of each H is described by a single coordinate pointing along the respective HB. Calling these single PT coordinates x_1 and x_2 two quartic potentials for the individual HBs are combined with a bilinear coupling term to give

$$U_{sym}(x_1,x_2) = \frac{U_0}{x_0^4}\left[\left(x_1^2-x_0^2\right)^2 + \left(x_2^2-x_0^2\right)^2\right] - \frac{gU_0}{x_0^2}x_1x_2 . \quad (8)$$

Here, x_0 is half the transfer distance for a single H atom and U_0 is the respective transfer barrier provided that the coupling strength parameter g is zero and the other H atom is fixed at x_0. Since DPT is usually discussed in terms of concerted and stepwise transfer, this potential is more conveniently expressed by using the symmetric and asymmetric transfer coordinates $x_s = (x_1 + x_2)/2$ and $x_a = (x_1 - x_2)/2$, respectively. This gives the potential (neglecting constant terms)

$$U_{sym}(x_s,x_a) = \frac{U_0}{x_0^2}\left[(g-4)x_a^2-(g+4)x_s^2\right] + \frac{2U_0}{x_0^4}\left(x_s^4+x_a^4+6x_s^2x_a^2\right). \quad (9)$$

This equation defines a 2D PES having two minima along the x_s coordinate if x_a is zero and *vice versa*. The minima along x_s correspond to the two *trans* configurations separated by a second order transitions state at (0,0), whereas the two minima along x_a are the *cis* configurations connected via the same second order transition state. Furthermore, there are four first order transition states separating *trans* and *cis* minima. The locations and energies of these stationary points are given by simple analytical expressions.[60]

The PES discussed so far describes symmetric molecules only. Recently, we have proposed a generalization to the case of asymmetric DPT systems. Two types of asymmetry can be introduced into the model Hamiltonian, that is, a detuning with respect to the *trans* and the *cis* configurations. Labeling the respective detuning parameters as α_{trans} and α_{cis}, asymmetry is modeled by the potential

$$U_{\text{asym}}(x_s,x_a) = \frac{U_0}{x_0}\left(\alpha_{\text{trans}}x_s+\alpha_{\text{cis}}x_a\right) . \quad (10)$$

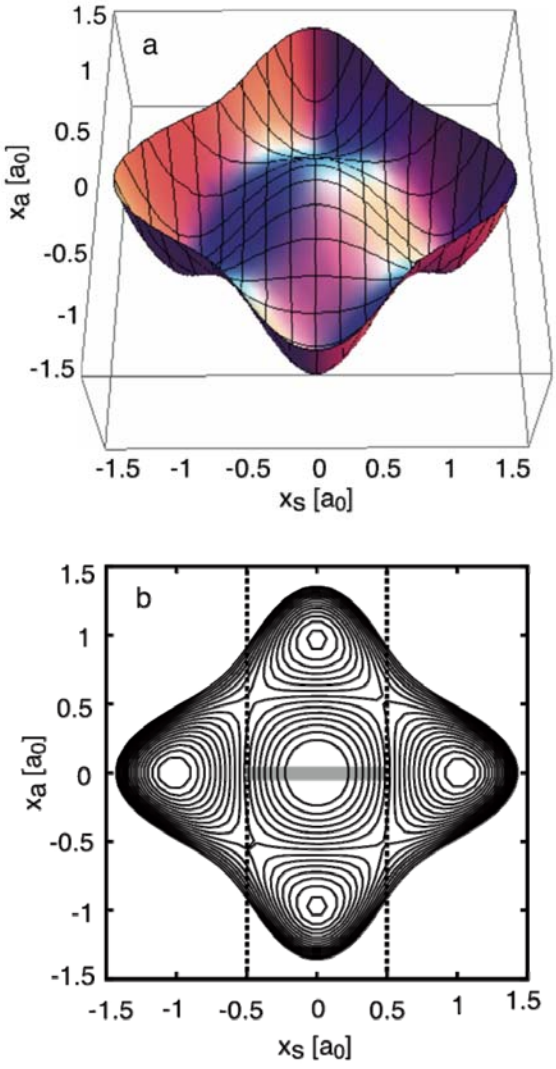

Figure 3. PES describing DPT in an asymmetric system according to Equations (9) and (10). The lower panel contains the definitions of concerted (shaded) and step-wise (in between dashed lines except in the shaded area) regions of the PES. Parameters: $U_0 = 2000$ cm^{-1}, $x_0 = 1.0\ a_0$, $g = 0.2$, $\alpha_{trans} = 0.005$, and $\alpha_{cis} = 0.0$. (contours in panel b from 0.05 to 0.9 in steps of 0.05 in units of the second order transition state energy 4428 cm^{-1}).

An example for an asymmetric 2D model PES describing DPT is shown in Figure 3. Taking everything together the total 2D DPT Hamiltonian is given by (m_H is the H mass)

$$H_0 = -\frac{\hbar^2}{4m_H}\left(\frac{\partial^2}{\partial x_s^2}+\frac{\partial^2}{\partial x_a^2}\right)+ \\ +U_{sym}(x_s,x_a)+U_{asym}(x_s,x_a)\ . \quad (11)$$

This model Hamiltonian can be used for the simulation of laser control of DPT as well. To this end it has to be supplemented by a molecule-laser field coupling term, which is usually taken in dipole approximation with $\boldsymbol{\mu}(x_s,x_a)$ being the dipole operator. For the sake of simplicity one can assume that the permanent dipole moment depends only linearly on the coordinates, i.e.,

$$H_{field}(t) = -(\mu_s x_s + \mu_a x_a)E(t). \quad (12)$$

Here the derivatives of the dipole moment with respect to x_s/x_a are introduced as μ_s/μ_a. Further, as before (*cf.* Equation (4)) it is assumed that the dipole moment vector is aligned with the polarization direction of the linearly polarized field. In the special case of symmetric DPT systems like porphycene the dipole moment will change along the asymmetric coordinate only.

2. 3. Time-Dependent Schrödinger Equation

In the following we will briefly sketch the solution of the time-dependent Schrödinger equation for a PT or DPT system driven by some control laser field. For simplicity we consider the case of two coordinates, q_1 and q_2. In this case the equation to be solved reads

$$i\hbar\frac{\partial}{\partial t}\Psi(q_1,q_2,t) = \left[H_0 + H_{field}(t)\right]\Psi(q_1,q_2,t). \quad (13)$$

A powerful method for the numerical solution is the multi-configuration time-dependent Hartree (MCTDH) approach[62,63] as implemented in the Heidelberg program package.[64] Here, the 2D wave function is expanded in a time-dependent basis of single particle functions $\{\varphi_j\}$ (SPFs) according to

$$\Psi(q_1,q_2,t) = \sum_{j_1=1}^{n_1}\sum_{j_2=1}^{n_2} A_{j_1 j_2}(t)\varphi_{j_1}(q_1,t)\varphi_{j_2}(q_2,t)\ . \quad (14)$$

The numerical saving as compared to the standard stationary basis set expansion results from the fact that the time-dependent basis is capable of adapting to the moving wave packet, thus giving a rather compact representation of the latter. This makes the required numbers of SPFs n_1 and n_2 smaller than for a static basis. The SPFs themselves are expanded into a so-called primitive basis $\{\chi_i\}$ within a truncated N-dimensional Hilbert space

$$\varphi_j(q,t) = \sum_{i=1}^{N} C_{ij}(t)\chi_i(q). \quad (15)$$

For numerical convenience one typically chooses a pseudospectral representation in terms of localized functions such as provided, for instance, by the discrete variable representation (DVR) method (for an overview, see Ref. 65).

In passing we note that the 2D Schrödinger Equation (13) could, of course, also be solved by the standard method, i.e. employing a stationary basis for the field-

free case obtained, e.g. using the FGH method. The full advantage of the MCTDH approach comes to its right only for real multidimensional quantum problems (for a recent compilation of examples including PT, see Ref. 66).

3. Strategies for Laser Control

The external laser field is usually given by

$$E(t) = E_0 s(t) \cos(\omega t + \varphi) \tag{16}$$

with amplitude E_0, envelope $s(t)$, carrier frequency ω, and carrier envelope phase (CEP) φ. In the following the field will be assumed to be polarized along the dominant component of the molecular dipole moment.

For the laser-driven dynamics a certain target state is defined, which should be reached from the initial ground state within a certain time T by choosing an appropriate laser field. Here, one can resort, for instance, to predefined parameterized laser fields. A common example would be pulse sequences composed of Gaussian or $\sin^2$-shaped pulses.[5,50] The optimization of the pulse parameters may be guided by the so-called π-pulse condition, where the system is driven through a number of quasi two-level system transitions from the initial to the final state. For a resonant laser pulse of duration T the condition

$$E_0 \mu_{10} \int_0^T dt\, s(t) = \pi \tag{17}$$

leads to a complete population inversion in a two level system if μ_0 is the dipole matrix element.[67] In a multilevel system, however, due to coupling between the vibrational levels the above condition provides only an initial guess for a laser pulse whose parameters need to be re-optimized using some search algorithm.

Laser pulses that are less biased towards a specific predefined form (and hence a guessed reaction path) and more adapted to the nuclear dynamics can be obtained from OCT. In its simplest version a functional J is defined, which is maximized at a final time T. Given an operator O describing the target state, e.g., a projection operator onto a certain eigenstate of H_0, i.e. $O = |\phi_{tar}\rangle\langle\phi_{tar}|$, this functional reads [68,69]

$$J = \left|\langle \Psi(T) | \phi_{tar} \rangle\right|^2 - \alpha \int_0^T dt \frac{E^2(t)}{s(t)} - \\ -2\,\mathrm{Re}\langle \Psi(T) | \phi_{tar} \rangle \int_0^T dt \langle \Phi(t) | \frac{\partial}{\partial t} + i(H_0 - \mu E(t)) | \Psi(t) \rangle \tag{18}$$

where α is the so-called penalty factor weighting the constraint on the field strength, $s(t)$ is some smooth shape function, and the function Φ(t) takes the role of a Lagrangian multiplier. Variational optimization leads to a set of equations, which give the optimized field by means of an iterative procedure.

$$E(t) = \frac{s(t)}{\alpha} \mathrm{Im} \langle \Psi(T) | \phi_{tar} \rangle \langle \Phi(t) | \mu | \Psi(t) \rangle . \tag{19}$$

We note that in deriving Equation (19) terms proportional to $\delta(E(t))^2$, useful when dealing with complex targets, have been neglected.[70] In passing we note that the iterative optimization of the field has been implemented within the MCTDH program package by Brown and coworkers[71] and therefore can be performed for multidimensional PES.

A characterization of the pulse, i.e. its temporal behavior and spectral content can be obtained by calculation of the so-called XFROG trace[71]

$$I_{XFROG}(\omega, t) = \left| \int_0^T d\tau\, e^{-i\omega\tau} E(\tau) G(\tau - t) \right|^2 , \tag{20}$$

where $G(t)$ is some gate function.

Next we focus on the laser-matter interaction in the ultrashort pulse domain, i.e., in the regime where the duration of the pulse is comparable to the oscillation period of the carrier light (see Figure 7). Under such conditions the assumption of a laser pulse consisting of a time-dependent envelope and a carrier wave of frequency ω is not valid anymore. Specifically, one needs to enforce the zero-net-force condition[18,19]

$$\int_0^T dt\, E(t) = 0 , \tag{21}$$

which ensures that the laser field is the solution of the Maxwell equation in the propagation region. The simplest way to account for the zero-net-force condition is to formulate the problem in terms of the vector potential

$$A(t) = -\frac{E_0 c}{\omega} s(t) \sin(\omega t + \varphi) \tag{22}$$

and to obtain the electric field as its time derivative

$$E(t) = -\frac{1}{c}\frac{\partial A(t)}{\partial t} = \\ E_0 s(t) \cos(\omega t + \varphi) + \frac{E_0}{\omega}\frac{ds(t)}{dt} \sin(\omega t + \varphi) . \tag{23}$$

The first term corresponds to the "traditional" radiation pulse having a bell-shaped envelope function, $s(t)$, a monochromatic carrier wave of frequency ω, and a CEP φ. The second term, containing the time derivative of the pulse envelope is negligible for many-cycle pulses, but becomes important in the sub-one-cycle pulse limit as shown in Figure 4.

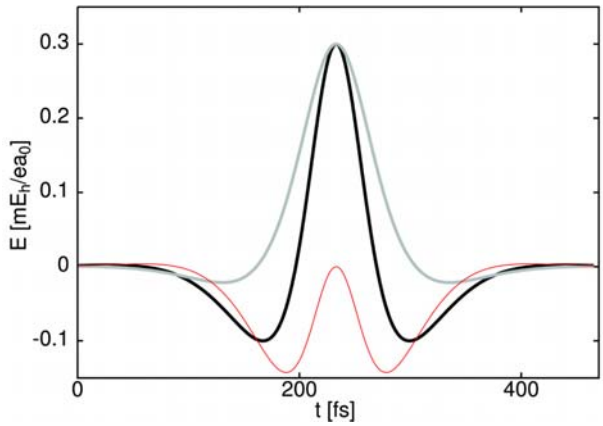

Figure 4. An ultrashort pulse with $n_c = 1/3$ and CEP $\varphi = 0$. The total electric field of the pulse (black) is compared with its two components: the "traditional" pulse consisting of an envelope and cosine carrier field (gray) and the time derivative of the pulse envelope with a sine carrier field (red, thin).

Following Brabec and Krausz the time-dependent envelope function $s(t) = \mathrm{sech}(t/\alpha)$ is used, which is centered at $t = 0$ with $\alpha_{1/2} = \alpha \ln(2 + \sqrt{3})$ being the half-width of the pulse at half-maximum (HWHM).[72] An ultrafast pulse can be characterized by the number of carrier wave oscillations, contained within the pulse width, n_c, measured at half the maximum $\alpha_{1/2} = n_c T = n_c/\omega$. In Figure 4 we display the time variation of the total electric field of an ultrashort, $n_c = 1/3$ pulses with CEP $\varphi = 0$ (cosine-pulse) together with the two field components specified by Equation (23). One notices that the inclusion of the envelope function derivative results in an effective increase of the pulse frequency by [18]

$$\delta = \omega\left(1 - \frac{1 + m_c^2\pi^2}{\sqrt{3 + 4m_c^2\pi^2 + m_c^4\pi^4}}\right) \tag{24}$$

with $m_c = n_c / \ln(2 + \sqrt{3})$. This effective increase of the pulse frequency is a key feature for the laser control of PT transfer in the ultrashort pulse domain.[19]

The zero-net-force condition can be straightforwardly incorporated in the framework of OCT by introducing a penalty factor, λ, that weights the magnitude of the direct-current (DC) component, Equation (21). The optimal field, Equation (19), is modified according to[19]

$$E(t) = -\frac{s(t)}{\alpha}\left[\mathrm{Im}\left\langle\Psi(T)\middle|\phi_{\mathrm{tar}}\right\rangle\left\langle\Phi(t)\middle|\mu\middle|\Psi(t)\right\rangle + \lambda\right]. \tag{25}$$

4. Results and Discussion

4. 1. Single Proton Transfer

In the following some examples of laser controlled single PT will be discussed, which serve as an illustration of the concepts introduced in Sections 2.1 and 3. As a model the enol to enethiol tautomerization in thioacetylacetone will be considered (cf. PES and eigenstates in Figure 2). Since in thermal equilibrium both tautomers are populated, we chose a thermal population of the eigenstates of the unperturbed Hamiltonian H_0, the so-called zero-order states, as our initial condition. In the π-pulse scheme the population inversion between the ground and first excited state can be obtained either by employing a third state that is coupled via a large transition dipole moment to both the initial and the final state in a pump-dump fashion or by direct transition between the initial and target state. In the latter case one takes advantage of the fact that the barrier for electronic ground state isomerization in thioacetylacetone is low and the dipole matrix element between the lowest vibrational states μ_{10} is nonzero.

Figure 5 displays the results of applying a $\phi_0 \rightarrow \phi_8 \rightarrow \phi_1$ pump-dump like pulse sequence.[12] The two pulses have been optimized by means of a simple searching algorithm starting from two overlapping π-pulses. The population dynamics of all involved zero-order states indicates that the intermediate state gets considerably populated during the interaction time, and it is not completely depopulated at the end of the pulse sequence. The resulting isomerization yield is approximately 85%.[12]

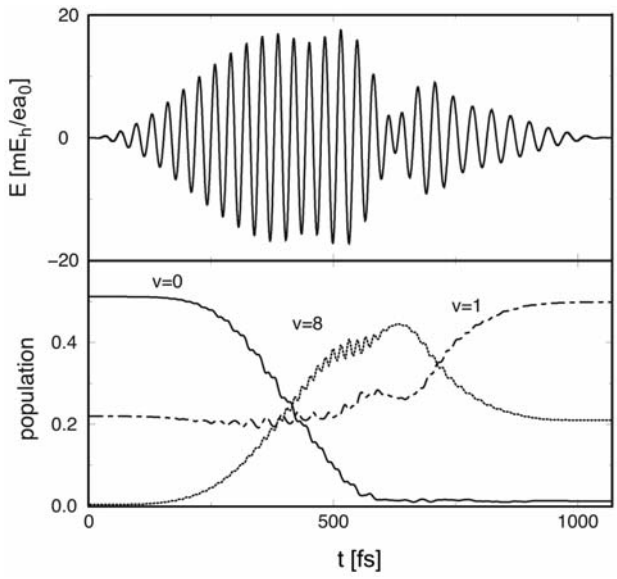

Figure 5. Upper panel: The laser field optimized for the pump-dump approach to laser controlled PT in the PES shown in Figure 2. Lower panel: population dynamics of these three states (for more details, see Ref. 12).

Tuning the pulse frequency into resonance with the $\phi_0 \rightarrow \phi_1$ transition and following the π -pulse criteria for a pulse with a Gaussian envelope one finds that the laser pulse shown in Figure 6, having a duration of 1300 fs, induces an almost complete population switch in the sys-

tem.[16] The direct resonance approach has considerable advantages with respect to the pump-dump approach:

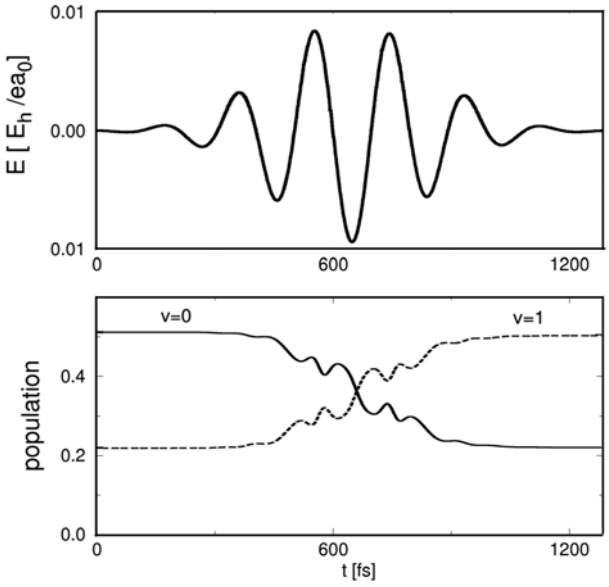

Figure 6. The laser field that is tuned in resonance with the $\phi_0 \rightarrow \phi_1$ excitation (upper panel) and the population dynamics of the two lowest eigenstates (lower panel) of a model for the tautomerization in thioacetylcetone (for more details, see Ref. 16).

it has a simple form, it requires a lower intensity of the laser field, and it does not involve the population of vibrationally excited states, which will be subject to faster vibrational energy relaxation.

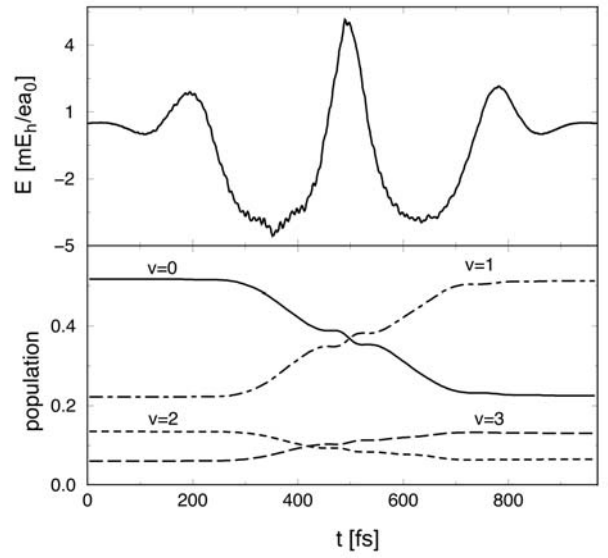

Figure 7. Upper panel: The laser field generated by OCT with a high penalty factor ($\alpha = 30$) for the model of Figure 2. The main frequency component of the pulse ($\omega = 88$ cm^{-1}) is lower than the energy difference between the initial and target state. Lower panel: The population dynamics is shown for the four lowest vibrational eigenstates during the isomerization reaction (for more details see Ref. 12).

Turning to OCT and imposing a high penalty for the field, i.e., allowing for moderate field intensities only, a completely different control mechanism is obtained. One of the resulting laser pulses is shown in Figure 7. It achieves a complete control over the system dynamics with a yield of 99%. Yet, the dominant frequency component of the pulse of $\omega = 88$ cm^{-1} is lower than the energy difference between the initial and final states which is $\omega_{10} = 176$ cm^{-1}.

The population inversion is achieved by a combined effect of tunneling and direct $\phi_0 \rightarrow \phi_1$ excitation. On the basis of the OCT result and mechanistic studies in the dressed molecular state representation, it becomes apparent that one could design a multitude of low-frequency pulses capable of achieving population inversion. In the extreme case the population inversion in a double well potential can be driven by a rectangular pulse consisting of switch-on – tunneling – switch-off periods[11] or by a half cycle-pulse as the one shown in Ref. 13.

The above results clearly indicate that laser control of intra-molecular PT can be obtained by following different mechanisms, from a π-pulse scheme employing a pump-dump mechanism or a direct resonant transition to laser induced tunneling. However, a detailed analysis points to a certain sensibility of the isomerization yield with respect to the pulse characteristics. To elaborate further on this issue one can investigate the dependence of the target state population on the field intensity, frequency and phase of the driving pulses.[73] The results are shown in Figure 8. The laser field amplitude varies in a uniform way between $-0.025 \leq E_0 \leq 0.025$ E_h/ea_0 with an increment of $\Delta E_0 = 0.5$ mE_h/ea_0 and the frequency varies between $0 \leq \omega \leq 245.8$ cm^{-1} with an increment of $\Delta\omega = 0.8$ cm^{-1}. Note that negative E_0 values correspond effectively to a CEP of $\varphi = \pi$. The duration of the laser pulses having a Gaussian envelope has been fixed to 1300 fs. For subpicosecond pulse durations appreciable population transfer occurs only via laser driven tunneling. However, the range of parameters for which efficient population transfer is achieved ($P_1 \geq 0.8$) is restricted due to the fact that for non-optimal pulses the dressed eigenstates get close to each other for a period shorter than the required tunneling time. From Figure 8 it is apparent that the reaction yield is larger than $P_1 = 0.8$ for a range of parameters satisfying only approximately the resonant π-pulse condition. In the off-resonance areas, efficient control is restricted to narrow parameter ranges.

Moreover, in the low-frequency areas a pronounced phase sensibility can be inferred from the difference in the target state probability between positive (right) and negative (left) field intensities corresponding to an effective change of the CEP from $\varphi = 0$ to $\varphi = \pi$. For example two areas of control with reaction yields higher than $P_1 = 0.8$ appear for $E_0 = -10$ mE_h/ea_0, $\omega = 105$ cm^{-1} and for $E_0 = -20$ mE_h/ea_0 and $\omega = 127$ cm^{-1} while no appreciable control has been achieved in the corresponding $\varphi = 0$ areas. In

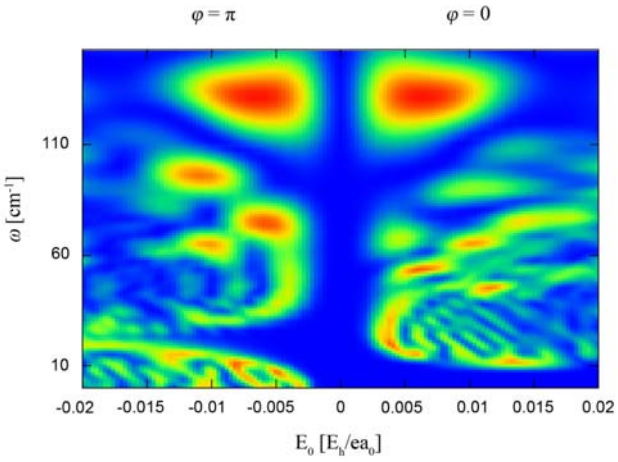

Figure 8. Target state population at the end of a 1300 fs Gaussian pulse excitation for the model of Figure 2. The variation of the final population is shown as a function of the electric field strength and the pulse frequency. The CEP are φ = 0 and φ = π.

the tunneling region the amplitude of the tunneling pulse E_0 can be calculated as $E_0 = \omega_{10}/(\mu_{00}-\mu_{11})$. Hence, in order to compensate for a negative value of $\mu_{00}-\mu_{11}$ the tunneling field has a negative amplitude or equivalently a CEP phase of $\varphi = \pi$. Phase sensitivity arises also from the complexity of the laser driven dynamics involving multiple population transfer between the initial and target state occurring at high field intensities. Moreover, during the excitation a large number of states get populated giving rise to the pronounced phase sensitivity.[73]

Let us now consider the control of the PT (H-atom transfer) in acetylacetone. The 3D PES spanned by internal, non-orthogonal coordinates has been introduced in Sec. 2, Equation (6). As in the case of thioacetylacetone, the laser control of the population transfer from the ground state ϕ_0 to the first excited state ϕ_1 corresponds to switching from the reactant to the product well. The two lowest levels are split by $\omega_{10} = 116$ cm^{-1}, the third and fourth states are split by $\omega_{32} = 182$ cm^{-1}, while the energy difference between the second and third state is $\omega_{21} = 222$ cm^{-1} cm^{-1}. Inspection of the dipole moment matrix elements reveals strong coupling between the adjacent doublets that may influence the selectivity of the laser driven transition. Figure 9 displays several high efficiency laser pulses with time durations between 450 and 1050 fs.[19] In this simulation the penalty for the DC component was set to $\lambda = 0.1$. It is apparent that all pulses have an absolute phase of $\varphi = \pi/2$. We note that these sine-type pulses were obtained irrespectively of whether cosine- or sine-pulses were used as initial guess. The pulses appear to be a superposition of two pulses: a longer one with $\varphi = \pi/2$, and a shorter one centered at around the minimum of the second lobe

The mechanism of the pulse action can be understood by analyzing the population dynamics of the involved zero-order states.[19] Figure 10 compares the action of a

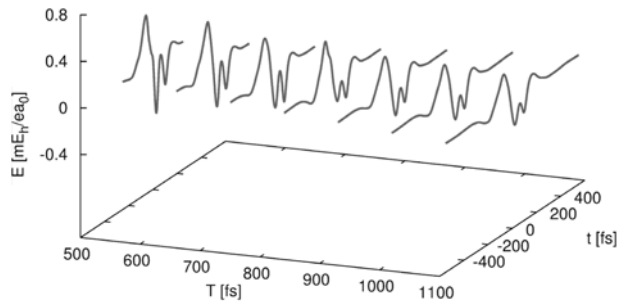

Figure 9. The variation of the electric field for several optimal control theory pulses obtained from Equation (25) for a model of acetylacetone. Pulse duration range from 500 to 1100 fs in steps of 100 fs. (for more details, see Ref. 19).

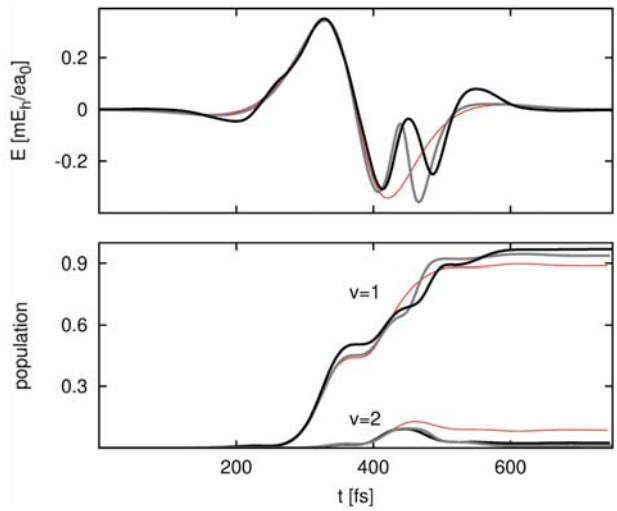

Figure 10. Upper panel: Three control pulses with *sech*-type envelope and duration of 750 fs for a model of acetylacetone: OCT pulse (black), monochromatic π-pulse with $n_c = 1/3$ (red, thin), and composed pulse (gray) obtained as a superposition of two $n_c = 1/3$ pulses with $E_{0,1} = 0.37$ mE$_h$/ea$_0$, $\omega_1 = 76$ cm^{-1} , and $E_{0,2} = 0.25$, $\omega_1 = 149$ cm^{-1}. The center of the second pulse is at 450 fs. Lower panel: Time-dependent population of the target state ϕ_1 and the background state ϕ_2 (for more details, see Ref. 19).

simple 750 fs pulse with sine-phase, and a frequency shifted to 72.9 cm^{-1} to account for its $n_c = 1/3$ pulse duration with respect to the optimal pulse of the same duration, and a composed (hand-made) pulse simulating the OCT pulse. The optimal pulse achieves a target state population of $P_1 = 0.98$, while the monochromatic pulse achieves a target state population of $P_1 = 0.89$ with the remaining population mostly located in state ϕ_2 with $P_2 = 0.09$. Although both pulses have comparable P_2 populations at $t = 450$ fs, at the end of the OCT pulse the major part of population is successfully driven to the target state. The following composed pulse uncovers the mechanism of the OCT pulse. It contains an $n_c = 1/3$ pulse with $E_0 = 0.37$ mE$_h$/(ea$_0$) and $\omega = 76$ cm^{-1} that matches well the first lobe of the optimal control pulse. At the maximum of the ϕ_2 state population

at approximately 450 fs, a second $n_c = 1/3$ pulse with CEP $\varphi = \pi/2$ and frequency of $\omega = 149$ cm^{-1} is centered. The second pulse is effectively in resonance with the $\phi_1 \rightarrow \phi_2$ transition at 222 cm^{-1}, but the frequency has been corrected to compensate for its ultrashort duration according to Equation (24). The amplitude of the second pulse has been adjusted numerically. From the population dynamics shown in Figure 10 it is apparent that the role of the second sub-pulse is to correct the population leaking to the ϕ_2 state.

Finally, these mechanisms for driven PT can be placed in the broader context of laser control. The mechanism uncovered by OCT has a strong similarity with the control strategy proposed by Etinski *et al.* in which a superposition of pulses efficiently removes leaking to a strongly coupled background state.[74] In turn this is a variant of the counter-diabatic approach of Demirplack and Rice based on the analysis of the background state population.[75] Thus, the proposed π-pulse superposition mechanism can be viewed as a counterpart of these strategies in the ultrashort pulse domain.

4. 2. Double Proton Transfer

In the following we will illustrate laser control of DPT for the generic model, Equation (11), adapted to the case of a small detuning between the *trans* minima and no detuning between the *cis* minima (*cf.* Ref. 49). Further, it has been assumed that the dipole moment changes only along the asymmetric coordinate ($\mu_a = 1.0\ e$). In passing we note that in particular porphycene derivatives offer a tunability of the energetics of the PES over a wide range (see, e.g., Ref. 76). The 2D PES is given in Figure 3 (for parameters, see figure caption) and the initial state in Figure 11. Due to the small detuning it is mostly localized in the reactant's *trans* minimum.

The obtained MCTDH DPT dynamics can be analyzed by inspecting snapshots of the 2D probability distribution. Alternatively, projections onto certain eigenstates can be performed to yield their time-dependent population. Within the MCTDH approach eigenstates can be obtained using the so-called improved relaxation method.[77]

The optimized laser field is given in Figure 12a. It is capable of transferring 81% of the initial reactant popula-

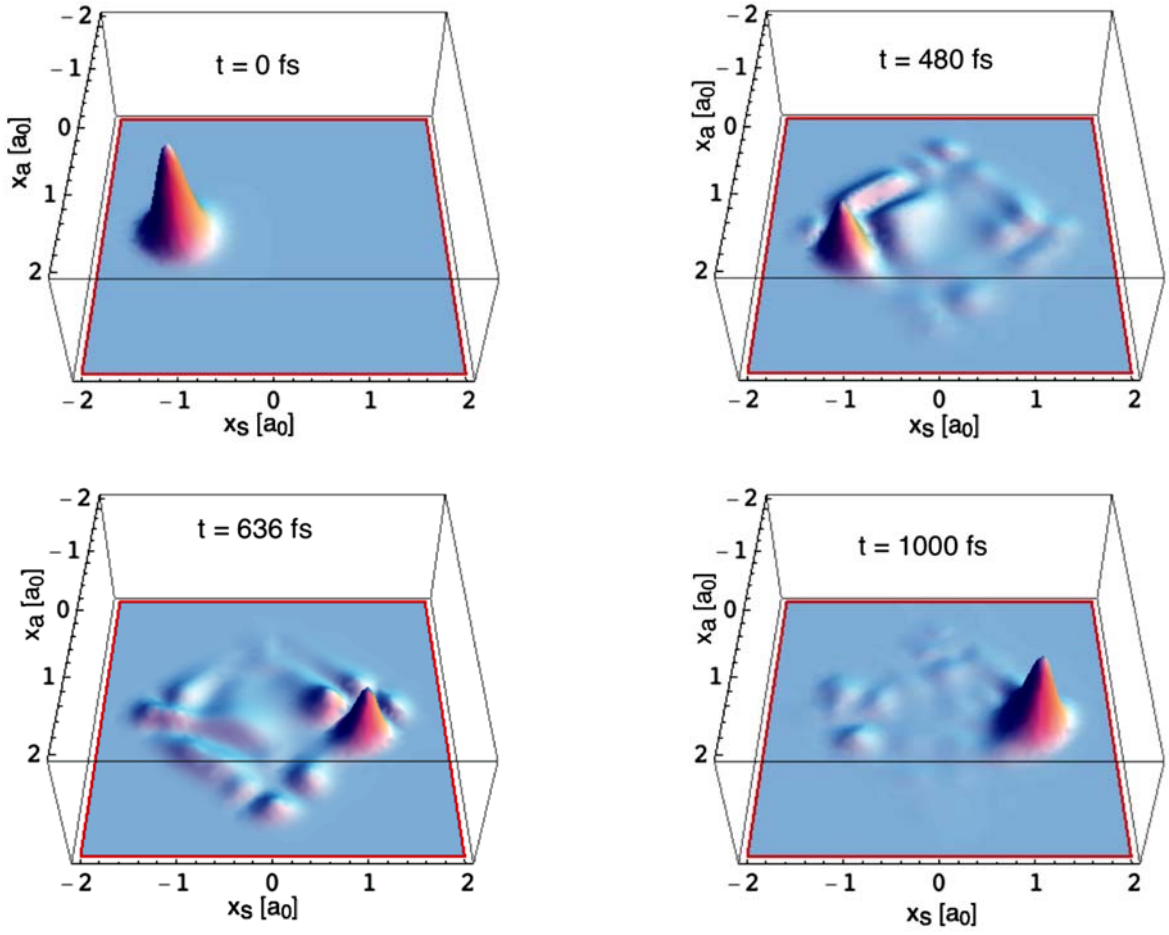

Figure 11. Laser-driven wave packet dynamics ($|\Psi(x_s,x_a,t)|^2$) of the model system shown in Figure 3. The two-dimensional wave function has been represented in both directions with a 64 point harmonic oscillator DVR on the interval $[-2.5.2.5]a_0$ and using 20 SPFs per coordinate. The $t = 0$ fs snapshot gives the initial state obtained by imaginary time-propagation. The final state at $t = 1000$ fs has a 81% overlap with the target state which is localized in the higher energetic *trans* minima. Intermediate snapshots have been selected to emphasize the transfer mechanism.

tion (P_0) to the product *trans* potential well. The respective eigenstate, which is mostly localized in that region, has been used as the target state (first excited state of the model Hamiltonian). The population dynamics of the initial and target states are shown in Figure 12c. Inspection of the snapshots taken from the wave packet dynamics (Figure 11) allows drawing the following conclusions. As a consequence of the coordinate dependence of the dipole moment, initially the system is excited along the x_a coordinate within the more stable *trans* potential well. With increasing strength the field drives the wave packet out of the *trans* well causing a delocalization. During most of the time evolution this delocalized wave packet covers most of the accessible configuration space of the system. Starting in the second half of the pulse, however, the field triggers a focusing of the wave packet into the product well region where it is finally localized.

The behavior of the wave packet is reflected in the population dynamics in Figure 12c, which can be understood in connection with the XFROG trace shown in Figure 12b. The latter reveals a pulse train, with partially overlapping sub-pulses having different frequencies. The first sub-pulse essentially depopulates the ground state by 50%. This depopulation is continued by the second subpulse, which is, however, red-shifted to facilitate efficient climbing to the next higher state. The latter is of mixed character, having contributions from local x_a and x_s excitations, being energetically in between the barrier for concerted and step-wise transfer (for details, *cf.* Ref. 49). The following sub-pulses populate even states being above the barrier for concerted transfer. At the same time, pulse-induced dumping of population into the product well starts to set in. It should be noted, that all sub-pulses have a broad spectrum, being essentially able to excite and deexcite several transitions simultaneously.

Since the mechanism of DPT is commonly classified as being either concerted (synchronous) or step-wise (asynchronous), a measure is needed to quantify the pathway on the basis of the time-dependent wave packet. In Ref. 49 it has been suggested to define certain ranges of the PES using step-like operators and take their expectation value as giving the probability for the respective mechanism. Figure 3b contains the definition of these ranges, which have, of course, a certain arbitrariness. For instance, one might call DPT as being concerted if the wave packet passes through a narrow range having the width of the ground state distribution (shaded area in Figure 3b). Wave packets going through the remaining range marked by the dashed lines are counted as a contribution to step-wise transfer. As a note in caution we emphasize that this does not imply the existence of a stable intermediate in the sense of traditional kinetics.

Looking at the wave packet dynamics in Figure 11 one would argue that a traditional classification in terms of concerted and step-wise DPT is not meaningful in the present case. Employing the measure introduced in Ref. 49 we notice from Figure 12d that most of the wave packet goes through the regions defined as step-wise, although the concerted pathway cannot be neglected, despite the rather narrow range for its definition (cf. Figure 3b).

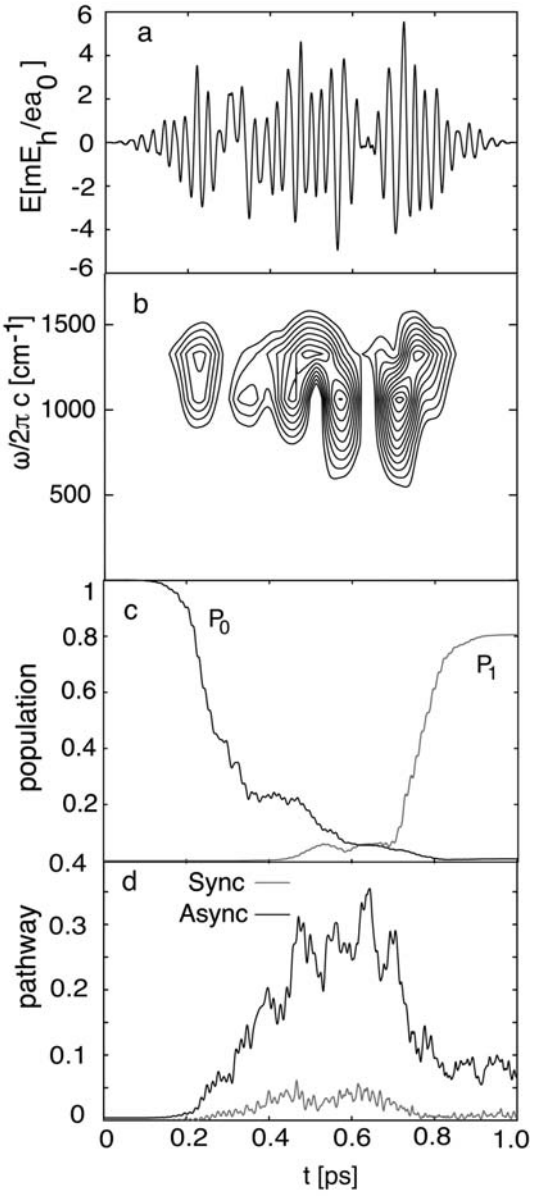

Figure 12. Results from an OCT calculation employing 224 iterations towards the goal to populate within $T = 1000$ fs the first excited state of the model Hamiltonian ($\alpha = 1.5$), which is localized in the product well. For the guess field which initiates the iterative optimization a sin-shaped envelope has been chosen together with a frequency of 1194 cm^{-1}, which corresponds to the fundamental excitation of the asymmetric vibration and $E_0 = 0.95$ mE$_h$/ea_0. (a) optimized laser field, (b) XFROG trace (Equation (20)) with contours at 1.8–5.8 a.u. in steps of 0.4 a.u., (c) population dynamics of initial (P_0) and target (P_1) state, (c) probability that wave packet is either in the synchronous or asynchronous transfer region (cf. Figure 3).

Finally, we would like to comment on an interesting side effect provided by the tool for controlling DPT reac-

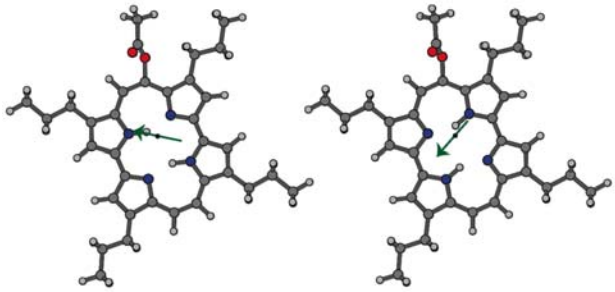

Figure 13. Two *trans* forms of tetra-n-propyleacetoxyporphycene and the orientation of the respective transition dipole moment vectors for the S_0–S_1 transition (for an experimental study of this system, see Ref. 78).

tions. Switching the positions of the two protons in the electronic ground state comes along with a change of the direction of the vector of the electronic transition dipole moment as shown exemplarily for a porphycene derivative in Figure 13.[50]

In order to appreciate this fact one has to recall that porphyrin-derivatives are used as chromophoric building blocks for molecular wires, which transport electronic excitation energy.[79] According to Förster theory the rate for excitation energy transfer between two chromophores depends on the relative orientation between their transition dipole moments.[80] For this reason controlling DPT has been suggested to be a means for designing a laser-triggered ultrafast switch built into an energy transfer molecular device.[50]

5. Conclusions

We have reviewed concepts, strategies, and methods for controlling proton or H-atom motion along single and double hydrogen bonds in the electronic ground state. Achieving control over proton transfer reactions is not only important from the conceptual point of view, but also as a platform for many applications. In spite of its relevance, the control of proton transfer reactions in the electronic ground state has yet to be reported experimentally. Our goal has been to identify the main obstacles to the control of proton transfer and to provide robust control strategies capable of achieving high reaction yields in complex molecular systems. Presently, this has been achieved by focusing on simple model systems. However, proton transfer is an intrinsically multidimensional chemical reaction in which quantum phenomena such as tunneling and zero point energy strongly influence the outcome. Hence, the control of proton motion requires having at hand adequate quantum chemical tools as well as the development of theoretical and computational methods of multidimensional quantum dynamics and laser control. We have outlined some strategies to go beyond simple low-dimensional models such as the MCTDH approach.

We have reviewed the ground state intra-molecular proton transfer in a two-dimensional model potential tailored to thioacetylacetone. It has been shown that the requirement of reducing the pulse intensity leads to a change in the underlying dynamics, i.e., from an above-barrier pump-dump type reaction to laser driven tunneling. Moreover, we have demonstrated that the outcome of the proton transfer reaction strongly depends on the carrier envelope phase of the driving pulse and that the experimental control of the phase of the laser pulses in the far IR region is a prerequisite for achieving efficient control. It can be anticipated that the tunneling mechanism of laser driven proton transfer remains unchanged when going from simple two-dimensional systems to coupled multidimensional system, and from simple analytical designed pulses to pulses generated by optimal control theory. The relative simplicity of the laser pulses that emerged from these studies indicate that it is possible to effectively confine the dynamics in a portion of the potential energy surface of reduced dimensionality, and in this way to diminish the competition with energy redistribution processes. Although these studies have focused on rather simple systems in the gas phase they provide an impetus for the control of PT in complex biomolecular systems interacting with different environments.

Further, we have shown that tailored laser fields obtained by optimal control theory can drive double proton transfer reactions with high efficiency. By using a two-dimensional potential that simultaneously allows for the concerted and step-wise double proton transfer, we have demonstrated that in laser-driven reactions the traditional distinction between synchronous and asynchronous proton transfer is removed. Thus, laser control is not only used to achieve a desired target state, but also as an analytical tool for investigating the ultrafast pathways of double proton transfer reactions. Finally, controlling double proton transfer may have an unexpected relevance for electronic transfer processes as has been demonstrated for the example of electronic excitation energy transfer in molecular photonic wires.

6. Acknowledgments

We gratefully acknowledge financial support by the DAAD and MZOŠ (098-0352851-2921) within a German-Croatian bilateral project.

7. References

1. D. Hadži (ed.), Theoretical treatments of hydrogen bonding, John Wiley and Sons, Chichester, **1997**.
2. J. T. Hynes, J. P. Klinman, H.-H. Limbach, R. L. Schowen (eds.), Hydrogen transfer reactions, Wiley-VCH, Weinheim, **2006**.

3. O. Kühn, L. Wöste (eds.), Analysis and control of ultrafast photoinduced reactions, Springer Series in Chemical Physics Vol. 87, Springer Verlag, Berlin, **2007**.
4. N. Došlić, Y. Fujimura, L. González, K. Hoki, D. Kröner, O. Kühn, J. Manz, Y. Ohtsuki, in F. C. De Schryver, S. De Feyter, G. Schweitzer (eds.), Femtochemistry, VCH-Wiley, Berlin, **2001**, p. 189.
5. O. Kühn, L. González, in Ref. 2, p. 71.
6. D. Hadži, *Pure Appl. Chem.* **1965**, *11*, 435.
7. K. Giese, M. Petković, H. Naundorf, O. Kühn, *Phys. Rep.* **2006**, *430*, 211.
8. S. Bratos, J.-C. Leicknam, G. Gallot, H. Ratajczak, in Ultrafast hydrogen bonding dynamics and proton transfer processes in the condensed phase, T. Elsaesser, H. J. Bakker (eds.), Kluwer Academic Publishers, Dordrecht, **2002,** p. 5.
9. N. Došlić, O. Kühn, J. Manz, *Ber. Bunsenges. Phys. Chem.* **1998**, *102,* 292.
10. M. V. Korolkov, J. Manz, G. K. Paramonov, *J. Chem. Phys.* **1996**, *105,* 10874.
11. N. Došlić, O. Kühn, J. Manz, K. Sundermann, *J. Phys. Chem. A* **1998**, *102*, 9645.
12. N. Došlić, K. Sundermann, L. González, O. Mó , J. Giraud-Girard, O. Kühn. *Phys. Chem. Chem. Phys.* **1999**, *1*, 1249.
13. H. Naundorf, K. Sundermann, O. Kühn, *Chem. Phys.* **1999**, *240*, 163.
14. O. Kühn, *Eur. Phys. J. D* **1999**, *6,* 49.
15. O. Kühn, Y. Zhao, F. Shuang, Y.-J. Yan, *J. Chem. Phys.* **2000**, *112*, 6104.
16. N. Došlić, O. Kühn, *Chem. Phys.* **2000**, *255*, 247.
17. N. Došlić, J. Stare, J. Mavri, *Chem. Phys.* **2001**, *269*, 59.
18. N. Došlić, *Phys. Rev. A* **2006**, *74*, 013402.
19. N. Došlić, *J. Phys. Chem. A* **2006**, *110*, 12400.
20. E. Geva, *J. Chem. Phys.* **2002**, *116*, 1629.
21. V. Engel, C. Meier, D. J. Tannor, *Adv. Chem. Phys.* **2009**, *141*, 29.
22. M. Ndong, D. Lauvergnat, X. Chapuisat, M. Desouter-Lecomte, *J. Chem. Phys.* **2007**, *126,* 244505.
23. Q. Ren, K. E. Ranaghan, A. J. Mulholland, J. N. Harvey, F. R. Manby, G. G. Balint-Kurti, *Chem. Phys. Lett.* **2010**, *491*, 230.
24. A. Douhal, S. K. Kim, A. H. Zewail, *Nature* **1995**, *378,* 260.
25. J. Catalán, P. Perez, J. C. del Valle, J. L. G. de Paz, M. Kasha, *Proc. Nat. Acad. Sci. USA* **2002**, *99*, 5793.
26. H. Sekiya, K. Sakota, *Bull. Chem. Soc. Jpn.* **2006**, *79*, 373.
27. S. Takeuchi, T. Tahara, *Proc. Nat. Acad. Sci. USA* 2**007**, *104,* 5285.
28. O.-H. Kwon, A. H. Zewail, *Proc. Natl. Acad. Sci. USA* **2007**, *104*, 8703.
29. J. Catalán, *Proc. Natl. Acad. Sci.* **2008**, *105,* E78.
30. O.-H. Kwon, A. H. Zewail, *Proc. Natl. Acad. Sci.* **2008**, *105*, E79.
31. H. Ushiyama, K. Takatsuka, *J. Chem. Phys.* **2001,** *115,* 5903.
32. L. Walewski, J. Waluk, B. Lesyng, *J. Phys. Chem. A* **2010**, *114*, 2313.
33. A. Accardi, I. Barth, O. Kühn, J. Manz, *J. Phys. Chem. A* **2010**, *114*, 11252.
34. J. Waluk, *Acc. Chem. Res.* **2006**, *39*, 945.
35. A. Vdovin, J. Waluk, B. Dick, A. Slenczka, *ChemPhysChem* **2009**, *10*, 761.
36. Z. Smedarchina, M. F. Shibl, O. Kühn, A. Fernández-Ramos, *Chem. Phys. Lett.* **2007**, *436*, 314.
37. J. M. Lopez del Amo, U. Langer, V. Torres, M. Pietrzak, G. Buntkowsky, H.-M. Vieth, M. F. Shibl, O. Kühn, M. Bröring, H.-H. Limbach, *J. Phys. Chem. A* **2009**, *113*, 2193.
38. G. V. Mil'nikov, O. Kühn, H. Nakamura, *J. Chem. Phys.* **2005**, *123,* 074308.
39. Z. Smedarchina, A. Fernández-Ramos, W. Siebrand, *J. Chem. Phys.* **2005**, *122*, 134309.
40. I. Matanović, N. Došlić, O. Kühn, *J. Chem. Phys.* **2007**, *127,* 014309.
41. M. Ortlieb, M. Havenith, *J. Phys. Chem. A* **2007**, *111,* 7355.
42. Y. Yan, O. Kühn, *J. Phys. Chem. B* **2011**, *115*, 4254.
43. M. F. Shibl, M. Pietrzak, H.-H. Limbach, O. Kühn, *ChemPhysChem* **2007**, *8,* 315.
44. M. Pietrzak, M. F. Shibl, M. Bröring, O. Kühn, H.-H. Limbach, *J. Am. Chem. Soc.* **2007**, *129,* 296.
45. K. Nishikawa, T. Ito, K. Sugimori, Y. Ohta, H. Nagao, *Int. J. Quant. Chem.* **2005**, *102*, 665.
46. I. Thanopulos, M. Shapiro, *J. Am. Chem. Soc.* **2005**, *127*, 14434.
47. I. Thanopulos, E. Paspalakis, V. Yannopapas, *Nanotechnology* **2008**, *19*, 445202.
48. I. Thanopulos, P. Kral, M. Shapiro, E. Paspalakis, *J. Mod. Opt.* **2009**, *56*, 686.
49. M. K. Abdel-Latif, O. Kühn, *Chem. Phys.* **2010**, *368*, 76.
50. M. K. Abdel-Latif, O. Kühn, *Theor. Chem. Acc.* **2011**, *128*, 307.
51. C. C. Marston, G. G. Balint-Kurti, *J. Chem. Phys.* **1989**, *91,* 3571.
52. J. Stare, G. G. Balint-Kurti, *J. Phys. Chem.* **2003**, *117,* 7204.
52. U. Berg, J. Sandström, L. Carlsen, F. Duus, *J. Chem. Soc., Perkin. Trans.* **1993**, *2,* 1321.
53. K. Giese, O. Kühn, *J. Chem. Phys.* **2005**, *123*, 054315.
54. I. Matanović, N. Došlić, B. R. Johnson, *J. Chem. Phys.* **2008**, *128,* 084103.
55. V. Alexandrov, D. M. A. Smith, H. Rostkowska, M. J. Nowak, L. Adamowicz, W. McCarthy, *J. Chem. Phys.* **1998**, *108*, 9685
56. J. Stare, *J. Chem. Inf. Model.* **2007**, *47*, 840.
57. I. Matanović, N. Došlić, *J. Phys. Chem. A* **2005**, *109*, 4185.
58. S. Bratož, D. Hadži, G. Rossmy, *Trans. Farad. Soc.* **1956**, *52*, 464.
59. Z. Smedarchina, W. Siebrand, A. Fernández-Ramos, *J. Chem. Phys.* **2007**, *127*, 174513.
60. Z. Smedarchina, W. Siebrand, A. Fernández-Ramos, R. Meana-Pañeda, *Z. Phys. Chem.* **2008**, *222*, 1291.
61. Z. Smedarchina, W. Siebrand, A. Fernández-Ramos, in Ref. 1, p. 895.
62. H.-D. Meyer, U. Manthe, L. S. Cederbaum, *Chem. Phys. Lett.* **1990**, *165*, 73.
63. M. H. Beck, A. Jäckle, G. A. Worth, H.-D. Meyer, *Phys. Rep.* **2000**, *324*, 1.

64. G. A. Worth, M. H. Beck, A. Jäckle and H.-D. Meyer, The MCTDH Package, Version 8.2, (2000), University of Heidelberg, Heidelberg, Germany, H.-D. Meyer, Version 8.3, (2002), Version 8.4, (2007). See http://mctdh.uni-hd.de.
65. D. J. Tannor, Introduction to quantum mechanics, University Science Books, Sausalito, **2007**.
66. H.-D. Meyer, F. Gatti, G. A. Worth (eds.), Multidimensional quantum dynamics: MCTDH theory and applications, Wiley-VCH, Weinheim, **2009**.
67. L. Allen, J. H. Eberly, Optical resonance and two-level atoms, Dover, Mineola, **1987**.
68. H. Rabitz, *Theor. Chem. Acc.* **2003**, *109*, 64.
69. K. Sundermann, R. Vivie-Riedle, *J. Chem. Phys.*, **2000**, *110,* 1896.
70. D. Geppert, R. de Vivie-Riedle, *Chem. Phys. Lett.* **2005**, *404*, 289.
71. M. Schröder, J.-L. Carréon-Macedo, A. Brown, *Phys. Chem. Chem. Phys.* **2008**, *10*, 850.
72. T. Brabec, F. Krausz, *Rev. Mod. Phys.* **2000**, *72*, 545.
73. I. Tatić, N. Došlić, *Croat. Chem. Acta.* **2004**, *77*, 83.
74. M. Etinski, C. Uiberacker, W. Jakubetz, *J. Chem. Phys.* **2006**, *124*, 124110.
75. M. Demirplak, S. A. Rice, *J. Phys. Chem. A* **2003**, *107*, 9937.
76. J. Waluk, in Ref. 2, p. 245.
77. H.-D. Meyer, F. Le Quere, C. Leonard, F. Gatti, *Chem. Phys.* **2006**, *329,* 179.
78. M. Gil, J. Jasny, E. Vogel, J. Waluk, *Chem. Phys. Lett.* **2000**, *323*, 534.
79. V. Balzani, A. Credi, M. Venturi, Molecular devices and machines, Wiley-VCH, Weinheim, **2003**.
80. V. May, O. Kühn, Charge and energy transfer dynamics in molecular systems, 3rd revised and enlarged edition, Wiley-VCH, Weinheim, **2011**.

Povzetek

V članku je prikazan pregled teorije in simulacije lasersko nadzorovane reakcije prenosa enega ali dveh protonov v molekulskih sistemih z vodikovo vezjo. Vpeljava različnih pristopov za formiranje ploskve potencialne energije omogoča oblikovanje enostavnih modelov, s pomočjo katerih spoznavamo osnovne mehanistične principe laserskega nadzora. Določanje polja kontrolnega laserja je osnovna naloga in opisanih je več metod, med njimi teorija nadzorovanega optimiranja. Uporaba je prikazana na primeru enoprotonskega prenosa s pomočjo infrardečega laserja v modelih tioacetilacetona in acetilacetona, pa tudi na primeru prenosa dveh protonov v derivatih porficena.